To appear in:

Journal of Theoretical and Applied Physics

Online ISSN: 2251-7235 **Print ISSN: 2251-7227**

DOI: 10.57647/jtap.2026.8604.0304
Research Article

Sensitivity Analysis of Toric and Multifocal IOL Optical Performance to Postoperative Tilt in the Presence of Corneal Aberrations

Maliheh Ranjbaran[1,2]*, Amirhesam Mehri[1,2], Mobina Sadat Marouf[1,2]

[1]*Department of physics, CT.C, Islamic Azad University, Tehran, Iran*
[2]*Institute of Biosocial and Quantum Science and Technologies, CT.C, Islamic Azad University, Tehran, Iran*

***Corresponding author:** ma.ranjbaran@iau.ac.ir

Received: 20 November 2025
Revised: 18 December 2025
Accepted:27 January 2026

ORCID: https://orcid.org/0000-0002-0984-0669

Abstract
Intraocular lenses (IOLs) are recognized as a solution in the treatment of eye conditions, particularly cataracts, by restoring vision through the replacement of the eye's natural lens. Selecting the appropriate type of IOL, based on individual patient characteristics such as corneal aberrations, plays a crucial role in the visual outcomes after surgery. This study assessed the efficacy of innovative diffractive multifocal and toric IOLs in treating visual impairment associated with corneal aberrations using computational modeling. The study examined how aberrations affected the quality of retinal images as measured by the modulation transfer function (MTF), peak-to-valley wavefront error, and root mean square (RMS) wavefront error. The results showed that contrast and resolution in near, intermediate, and far vision were much enhanced by optimized IOL designs. Postoperative IOL tilt cannot be predicted preoperatively; therefore, this study is framed as a sensitivity analysis evaluating how varying degrees of tilt affect optical quality across different IOL designs. Our simulations also revealed that IOL tilt negatively correlated with visual acuity, especially toric IOLs showing greater sensitivity due to increased tilt-induced astigmatism. Since this approach is tailored to the individual characteristics, the results support the development of IOL designs with improved tolerance to tilt-induced aberrations.

Keywords
Corneal Aberration, Zemax software, Liou-Brennan eye model, Diffractive multifocal IOLs, Toric IOLs, Shack-Hartmann sensor.

Introduction
Intraocular lenses (IOLs) are significant therapeutic modality in cataract, restoring vision by replacing the patient's natural eye lens [1]. The choice of IOL dramatically influences postoperative visual quality, depending on factors such as corneal aberrations [2] and the

sensitivity of the IOL to precise positioning [3] in the individual patient. Optimal selection of IOLs can significantly improve a patient's life and minimize the need for further corrective measures. In present-day choices, there are various kinds of IOLs, including monofocal [4,5], multifocal [6,7], toric [8,9], and aspheric [10, 11] lenses.

Monofocal IOLs are designed to provide optimal image quality at a single focal plane; however, the targeted focal distance can be selected based on patient needs, such as distance, intermediate, or near vision. Multifocal and extended depth-of-focus (EDoF) IOLs, in contrast, expand the range of functional vision by redistributing or extending optical focus. Depending on their optical design (e.g., bifocal, trifocal, or EDoF) and patient preferences, these lenses may be optimized for combinations of distance–near, distance–intermediate, or intermediate–near vision, thereby reducing dependence on spectacles for daily activities. Although these lenses may be associated with varying optical trade-offs, including reduced contrast sensitivity and photic phenomena such as glare and halos [12]. Toric IOLs are specifically designed to correct pre-existing corneal astigmatism, significantly improving vision in cataract patients with regular astigmatism by compensating for corneal cylindrical power [13]. Aspheric IOLs were developed to correct spherical aberration introduced by the cornea's shape, thereby improving retinal image quality, contrast sensitivity, and overall optical performance, particularly for larger pupil diameters [14].

IOL selection greatly impacts the quality of vision after surgery in patients with cataracts. Although postoperative IOL tilt is a well-recognized factor affecting visual quality, its magnitude and direction cannot be reliably predicted at the time of IOL selection. Factors such as capsular bag asymmetry, surgical technique, and postoperative capsular contraction contribute to tilt variability [15-17]. Consequently, computational modeling is best suited for evaluating the sensitivity of different IOL designs to potential postoperative misalignment. Also, Higher-order corneal aberrations (HOAs) play crucial roles in the choice of proper IOL type [18]. Studies indicate that these parameters can affect toric and multifocal IOLs performance and reduce the visual acuity or produce undesirable optical effects [19]. Al-Sayyari et al. conducted a comprehensive investigation highlighting the importance of considering corneal spherical aberration during the selection of IOLs for cataract surgery in maximizing visual outcomes and avoiding postoperative complications [2]. Also, studies have shown time-dependent changes in HOAs after surgery [20]. IOL decentration and tilt after surgery can also reduce the effectiveness of toric and multifocal IOLs. It is correlated with intermediate distance visual acuity [21]. Tilts of 2 to 3 degrees and decentrations of 0.2 to 0.3 mm are common, but they can negatively affect visual performance [22]. Toric IOLs are designed to correct astigmatism, but improper rotation can diminish their corrective effect [23]. Corneal aberration correction using diffractive IOLs was modeled in simulation research using Zemax software [24]. Lastly, studies using ray tracing method have assessed the astigmatism introduced by the IOL tilting [3].

Using a comprehensive ray-tracing simulation based on the Liou and Brennan eye model [25] implemented in Zemax software, this study investigated the effects of various IOL designs and their sensitivity to postoperative tilt on the correction of corneal aberrations. Aberrations at the retina were evaluated using a Shack-Hartmann wavefront sensor that was placed in front of the simulated lenses. Models of the IOLs' aspheric, toric, and binary-2 surfaces were created. Aspheric-binary 2 (diffractive multifocal) and aspheric-toroidal (toric) IOLs' corrective

performance was examined using modulation transfer function (MTF) diagrams, root mean square (RMS) wavefront error, and peak-to-valley wavefront error at the retina. Finally, Zernike polynomials were used to quantify the astigmatism induced by IOL tilt.

Materials and methods

Based on the Liou and Brennan model, this study used an accurate computational model of the human eye [25]. This model provides a thorough simulation of optical behavior by incorporating parameters for an ideal human eye, such as the shape, thickness, and refractive index of the cornea, aqueous, pupil, gradient crystalline lens, vitreous, and retina (as given in Table 1) [26]. Zemax ray-tracing software, a well-known tool for modeling optical systems, was used for the simulations. The eye has a refractive power of 60.35 diopters and is roughly represented by a sphere with an axial length of 23.95 mm in the Liou-Brennan model. The diameter of the pupil was fixed at 2.5 mm.

Table. 1. Lens data editor of Liou-Brennan eye model [29].

Surf: Type		Comment	Radius (mm)	Thickness (mm)	Glass	Semi-Diameter (mm)	Conic
0	standard	Object	Infinity	1000.000	-	0.000	
1	standard	Input Beam	Infinity	50.000	-	1.878	
2	standard	Cornea	7.770	0.550	1.38, 50.2	5.000	-0.180
3	standard	Aqueous	6.400	3.160	1.34,50.2	5.000	-0.600
4	standard	Pupil	Infinity	0.000	1.34,50.2	1.250	
5	Gradiant3	Lens-front	12.400	1.590		5.000	
6	Gradiant3	Lens-back	Infinity	2.430		5.000	
7	standard	Vitreous	-8.100	16.239	1.34,50.2	5.000	0.960
8	standard	Retina	-12.000	-	-	5.000	

Table 2 presents the parameters used to model the crystalline lens. The lens was simulated using a gradient 3 surface with a refractive index defined by the equation 1:

$$n = n_0 + n_{r_2}r^2 + n_{r_4}r^4 + n_{r_6}r^6 + n_{z_1}z + n_{z_2}z^2 + n_{z_3}z^3. \quad (1)$$

Table. 2. The parameters of gradient 3 surface

Surf: Type		Comment	n_0	n_{r_2}	nz_1	nz_2
5	Gradiant3	Lens-front	1.368	-1.978E-3	0.049	-0.015
6	Gradiant3	Lens-back	1.407	-1.978E-3	0.000	-6.605E-3

To simulate the corneal aberration in the software, the eye model remains identical to the previously used Liou and Brennan model. The only difference is that the cornea has been replaced with a paraxial surface possessing the same power and Zernike standard phase surface as given in Table 3. The Zernike phase surface type allows representation of the wavefront aberrations characteristics. The added phase to the rays was simulated using $\Phi = \sum_{i=0}^{N} A_i Z_i(\rho, \varphi)$. Each Zernike polynomial (Z_i) was weighted by a coefficient (A_i), with the normalized radial (ρ) and angular (φ) ray coordinates determining the value of each polynomial. The total number of polynomials used was N. The software used this formula to

define phase variations across the cornea, simulating the irregular shape and resulting optical path differences without directly modeling the physical surface deformation.

Table. 3. The modeled corneal aberration.

Surf: Type		Radius (mm)	Thickness (mm)	Glass	Semi-Diameter (mm)	Diffraction order	Focal length (mm)
2	paraxial	-	0.000	1.337, 52.66	5.000	-	23.174
3	Zernike standard phase	Infinity	2.074	1.337, 52.66	5.000	1	-

Advanced imaging techniques (corneal tomography, confocal microscopy, densitometry, and angiography) [27], clinical examination (visual acuity, refraction, slit-lamp biomicroscopy, corneal topography, and pachymetry) [28], and diagnostic instruments (wavefront aberrometry [29,30], Pentacam [31]) are all used in the diagnosis of corneal aberrations. While imaging offers comprehensive quantitative information on corneal shape and thickness, clinical evaluation detects distinctive symptoms such as irregular astigmatism and corneal thinning. Corneal aberration identification and monitoring are greatly aided by modern diagnostic instruments, such as the Shack-Hartmann wavefront sensor (used for wavefront aberration analysis) [32, 33].

In this study, After the eye simulation, a Shack-Hartmann sensor was designed to measure aberrations in both ideal and diseased eyes. The sensor's fundamental principle involves focusing a light beam (at near infrared) onto the retina, which acts as a diffuse light source. The weak reflected light then passes through various ocular components, each contributing to the wavefront's shape at the eye's exit pupil. As shown in Fig .1, the Shack-Hartmann sensor comprising two-telescope system, a lenslet array and an imaging sensor positioned at the lenslet focal plane, measures these wavefront distortions. The first telescope directly images the eye's pupil. A pinhole in the second telescope minimizes backscattered light while magnifying the image for lenslet array. The lenslet spatially measures the wavefront's deformation by evaluating the lateral focal shift on the imaging sensor. This measurement should not be interpreted as an absolute value, but rather as a relative deformation compared to a reference wavefront, typically a plane wave. The complete wavefront is then reconstructed from the data obtained from each lens. Zernike polynomials are used to quantify the various aberrations present in the eye [34, 35].

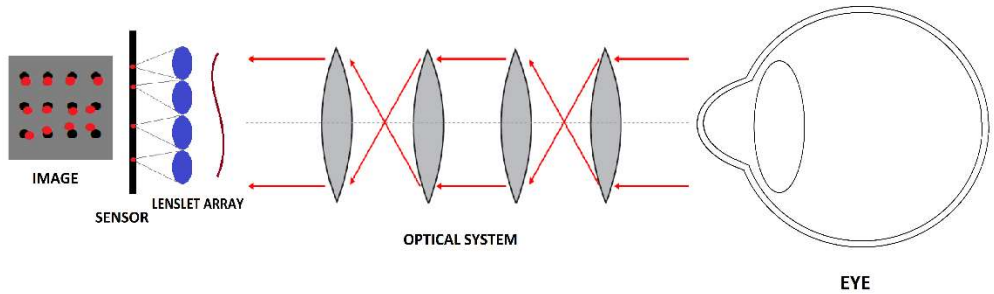

Fig. 1. Schematic diagram of Shack-Hartmann sensor in front of the eye.

In order to use IOL in the presence of corneal aberration, this paper explores the use of even asphere (aspheric) surfaces. Unlike traditional spherical IOLs, aspheric IOLs offer improved correction of corneal irregularities through variations in curvature. Spherical lenses often leave some higher-order aberrations, like coma and spherical aberration, uncorrected. Aspheric IOLs lessen these aberrations by more closely matching the eye's natural anatomy [36]. The Even asphere surface, deviating from a spherical shape, is calculated as:

$$Z(r) = \frac{cr^2}{1 + \sqrt{1 - (1+k)c^2\, r^2}} + \sum_{i=2}^{n} A_i\ r^{2i}, \qquad (2)$$

where Z(r) is the sag height at radial distance r from the optical axis, c is the curvature (1/radius), k is the conic constant, and A_i are the higher-order aspheric coefficients.

The aspheric surfaces can be combined with toroidal or diffractive surfaces, each offering distinct advantages. These IOLs are specifically designed to correct higher-order aberrations and improve visual acuity. This study simulated two intraocular lens (IOL) models. The first model used even-asphere and toroidal surfaces, as anterior and posterior surfaces of the lens, to represent a toric IOL. Unlike standard spherical IOLs, toric IOLs possess a cylindrical power component, allowing for precise correction of irregular astigmatism [37, 38]. The toroidal surface was defined by:

$$Z(y) = \frac{cy^2}{1 + \sqrt{1 - (1+k)c^2\, y^2}} + \sum_{i=2}^{n} A_i\ y^{2i}, \qquad (3)$$

where Z(y) describes the height (z) of a toroidal surface at any point (y,z). The curvature and conic shape are defined by parameters c and k, while the higher-order aspheric terms (α_i) further refine the surface's shape.

The second model simulated a diffractive multifocal IOL with an even-asphere surface and a Binary 2 diffractive surface. The Binary 2 surface's phase change was calculated using the equation:

$$\phi = M \sum_{i=1}^{N} A_i\ \rho^{2i}, \qquad (4)$$

where N is the number of polynomial coefficients, ρ is the normalized radial distance, and M is the diffraction order. The modeled IOL corresponds to a trifocal diffractive design, in which near, intermediate, and distance foci are generated through controlled redistribution of incident light among diffraction orders. In the present model, light energy was distributed primarily between the zeroth and first diffraction orders, corresponding to distance and near/intermediate focal points, respectively. An approximately symmetric energy distribution (≈50% to the zeroth order and ≈50% to the first order) was assumed, consistent with non-apodized diffractive multifocal IOL designs [39].

In our simulations, visual performance was evaluated at three focal distances: far (object at infinity), intermediate (object at 1000 mm), and near (object at 500 mm). To model off-axis viewing and simulate gaze direction toward objects at these distances, the eye model was tilted around the x-axis by 0°, -10°, and -20°, respectively.

To improve the optimization of aberrations generated by the designed IOL, merit functions such as MTFT (tangential modulation transfer function), MTFS (sagittal modulation transfer function), and MTFA (diffraction modulation transfer function, average of sagittal and tangential) were added, along with XNEG and XXEG (which represent minimum and maximum edge thickness), to the standard merit functions in ZEMAX software. Subsequently, various parameters, including the radius of the diffractive surfaces and the polynomial coefficients, were set as variables to carry out the optimization process.

Results and discussion

The Shack-Hartmann sensor's output shows an array of spots, each formed by the lenslet. The spot positions deviate from their ideal locations, mapping the wavefront aberrations caused by the eye's refractive errors. This spot pattern is then analyzed to quantify the wavefront's shape deformation. Fig. 2. represented the detected spot patterns and reconstructed wavefront maps of the ideal eye and the eye with corneal aberration. The sensor output revealed a conical shape in the diseased eye (Fig. 2. b and d) compared to the ideal eye (Fig. 2. a and c).

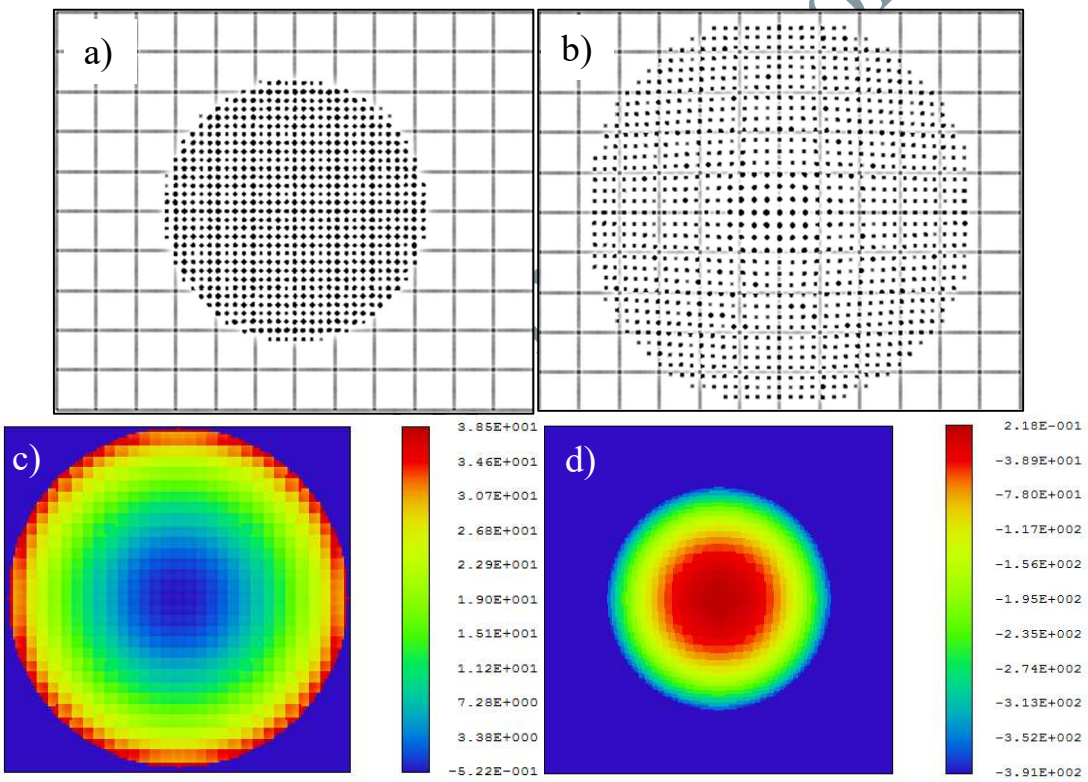

Fig. 2. Spot pattern at the output of Shack- Hartmann sensor for a) ideal eye and b) the eye with keratoconus. Wavefront maps of c) ideal eye and d) the eye with keratoconus.

Table 4 compares the peak-to-valley (P-V) and root-mean-square (RMS) wavefront aberrations in eyes with corneal aberration to those in ideal eyes. P-V and RMS values quantify the magnitude of wavefront distortion, representing the overall deviation from an ideal wavefront. The results demonstrate a statistically significant increase in both P-V and RMS values in eyes affected by corneal aberration, indicating substantially greater wavefront aberration.

Table. 4. Comparison of P-V and RMS wavefront aberrations in the ideal eye and the eye with corneal aberration.

	Peak to valley (waves)	RMS (waves)

Ideal eye	1.166	0.225
Eye with corneal aberration	391.221	108.175

Further analysis could investigate the different types of aberrations predominantly affected by corneal aberration. This could involve a detailed examination of the Zernike standard coefficients, given in Table. 5, derived from the wavefront maps to identify the specific aberration types contributing most significantly to the increased P-V and RMS values.

Table. 5. Comparison of Zernike standard coefficients in the ideal eye and the eye with corneal aberration.

	Z_1^1 (Tilt)	Z_2^0 (Defocus)	Z_2^2 (Astigmatism)	Z_3^1 (Coma)	Z_3^3 (Trefoil)	Z_4^0 (Spherical aberration)
Ideal eye	-0.037	0.043	0.020	-0.012	0.000	0.008
Eye with corneal aberration	0.043	2.562	0.028	0.015	0.000	-0.028

After the merit functions were determined, the optimization process was carried out to find the optimum polynomial coefficients and parameters of toric and multifocal IOLs, as shown in Table 6. The Binary 2 surface coefficients were defined using Zemax normalized radial coordinate $\rho = r/R_{\text{norm}}$. Consequently, the polynomial coefficients are scaled quantities and should not be interpreted as having direct physical units.

Table. 6. Parameters of designed toric and multifocal IOLs.

	Surf:Type	Radius (mm)	Radius of rotation (mm)	4th order term	6th order term	coeff. on ρ^2	coeff. on ρ^4	coeff. on ρ^6	coeff. on ρ^8
Toric IOL	Toroidal	439.678	-3.041 E+08	-	-	-	-	-	-
	Even asphere	-8.744	-	8.257 E-05	6.282 E-05	-	-	-	-
Multifocal IOL	Binary 2	14.941	-	1.070 E-04	-4.108 E-07	-1.057 E47	6.911 E34	-0.037	200.316
	Even asphere	-25.487	-	-5.047 E-04	6.071 E-05	-	-	-	-

The quality of the retinal image produced by the optimized toric and multifocal IOLs was evaluated using the spot diagrams for far, intermediate, and near visions in Fig. 3. These diagrams revealed a significant reduction in spot size for the treated eye compared to the untreated eye, from about 80 µm to 6-18 µm while Airy disk was about 4.3 µm. Improvements were significantly observed due to decrease in spherical and defocus aberrations.

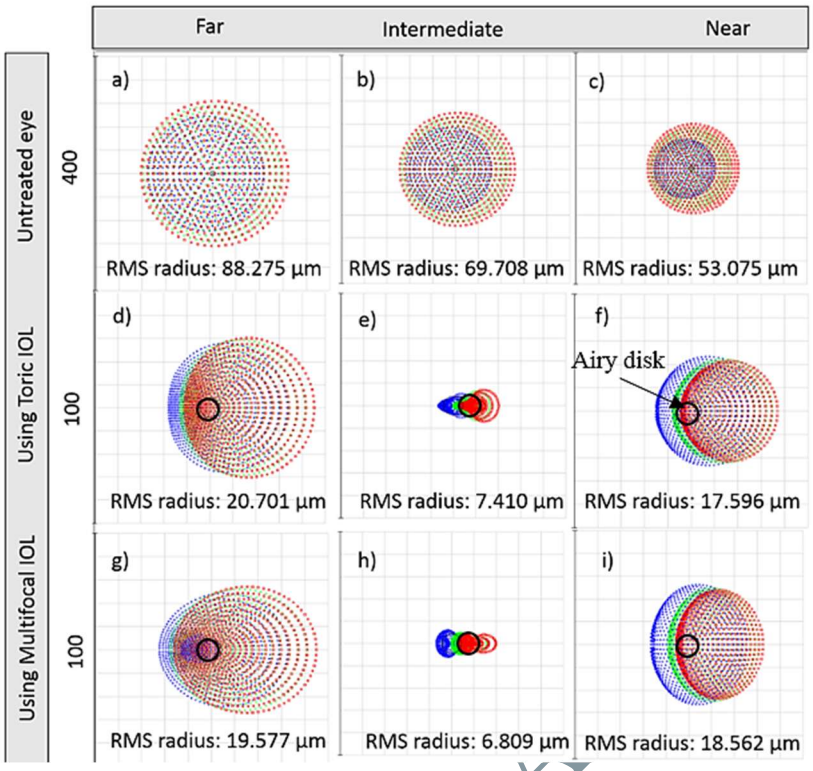

Fig. 3. The spot diagrams of untreated eye at a) far, b) intermediate, and c) near distances. The spot diagrams of treated eye with the designed toric IOL at d) far, e) intermediate, and f) near distances, and with the designed multifocal IOL at g) far, h) intermediate, and i) near distances.

Modulation Transfer Function (MTF) is another analysis that provides important information on the quality and sharpness of retinal images. Better contrast transfer and overall picture resolution are indicated by a higher MTF value. For the human eye to detect line differences, resolution must be more than 0.4, and the ideal spatial frequency for image resolution is 30 lines pairs per millimeter.

Improvements in image quality with treatment with both toric and multifocal IOLs are shown in Fig. 4, which displays MTF data. According to this figure, the toric lens improved contrast and resolution most notably in near and intermediate vision, suggesting that higher spatial frequencies were better transmitted. On the other hand, multifocal lenses demonstrated superior MTF at far distances. However, other factors like pupil size and IOL decentration can affect the outcome of treatment [40].

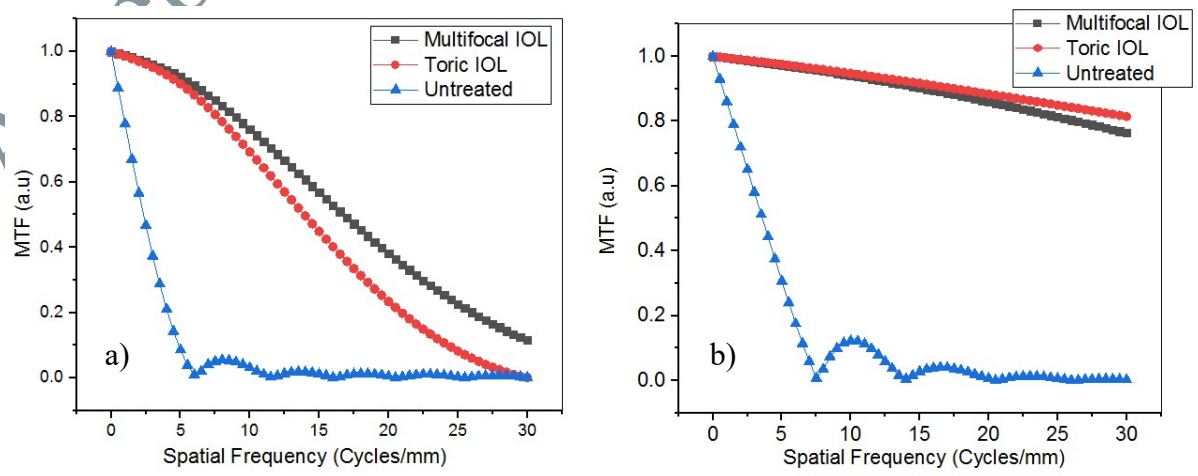

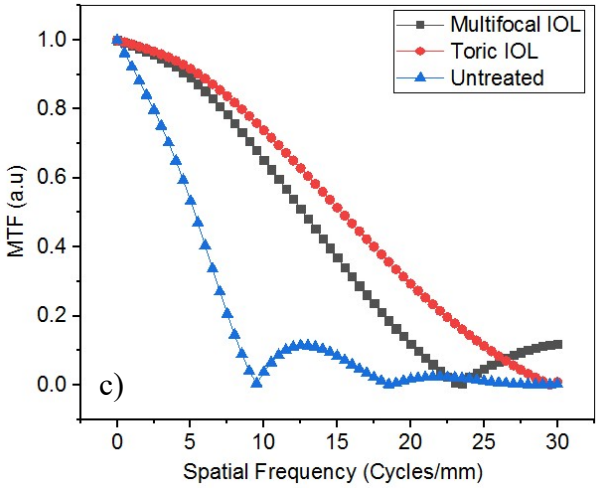

Fig. 4. The comparison of MTF diagrams at a) far, b) intermediate, and c) near distances.

Finally, the IOLs were rotated around the x-axis to replicate the tilt magnitudes reported in postoperative imaging studies, which typically range from 2° to 6° on average, with outliers up to 10° or more in cases of zonular weakness or capsular asymmetry [41,42].

To assess optical sensitivity to potential variations in IOL positioning during surgery, the simulation incorporated tilt angles ranging from 0 to 10°. The results demonstrated that increasing IOL tilt led to a loss in visual acuity, especially for toric IOLs, through elevated induced astigmatism (quantified via Z_2^2 Zernike standard coefficient). Using the equation $C = 4\sqrt{6}Z_2^2/R^2$,where R is pupil radius, the dioptric power of cylinder (C) was calculated and depicted in Fig. 5 as a function of IOL tilt [3, 40].

Our model suggests that for the 14 D designed toric IOL, a tilt about 10° may induce astigmatism greater than 0.3 D, which aligns with computational literatures [3]. Clinical studies verify this sensitivity in toric IOLs, where tilt intensifies astigmatism and higher-order aberrations (e.g., coma), potentially leading to induced cylindrical power [43,44]. Although the simulated tilt values should be interpreted as sensitivity analyses rather than predictions of clinical tilt magnitude.

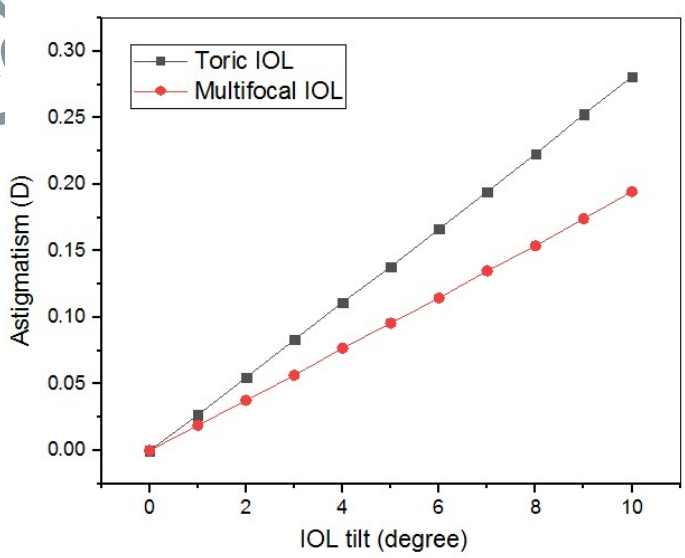

Fig. 5. The induced astigmatism as a function of IOLs tilts.

Although Shack–Hartmann sensors are commonly used for corneal wavefront measurement, they are not suitable for accurate aberration analysis of diffractive IOLs due to diffraction-induced phase discontinuities [45, 46]. Therefore, in this study, the Shack–Hartmann sensor was used only for corneal aberration evaluation, while the optical performance of diffractive IOLs was assessed using ray-tracing based simulations and Zernike analysis in Zemax software.

Conclusion

The Liou-Brennan eye model in Zemax software was used in this study to model both ideal eye and an eye with corneal aberration. To measure the aberrations, a Shack-Hartmann sensor was designed. Models of toric and multifocal IOLs were created by combining aspheric surfaces with toroidal and Binary 2 surfaces in the presence of corneal aberration. The MTF and spot diagram simulation results showed that the developed IOLs successfully decreased higher-order aberrations. The multifocal and toric IOLs effectively treated pre-existing corneal astigmatism while providing adjustments for near, intermediate, and far distance vision.

Reduced optical distortion, better low-light vision, increased contrast sensitivity, and a decrease in higher-order aberrations are some benefits of adopting toric and multifocal IOLs in cases with corneal aberration. The simulations' outputs also highlighted how important exact IOL placement is to getting the best possible visual results. Postoperative IOL tilt has a significant impact on induced astigmatism and may negate the desired aberration correction. Interestingly, it was discovered that toric IOLs were more sensitive to tilt-induced astigmatism than multifocal IOLs.

In order to improve visual acuity and minimize visual disturbances, this study emphasizes how important it is for surgeons to minimize IOL tilt during implantation. This sensitivity-based computational framework provides important information for surgeons and researchers, offering guidance for surgical planning and IOL design evaluation. However, this study was based on a simulated model of the human eye, which might not accurately represent the complexities of individual patient variations.

Disclosures

The authors declare no conflicts of interest.

Funding Declaration

No Funding.

Data Availability Statement

All input data for the simulations conducted in this study are available within the article.

References

[1] W. D. Joo, and M. S. Jung, “A study of optical properties of intraocular lenses and of measurement of the index of reflection for an unknown liquid”. *Journal of the Optical Society of Korea*, 16: 236-242, 2012. DOI: https://doi.org/10.3807/JOSK.2012.16.3.236.

[2] T. M. Al-Sayyari, S. M.Fawzy, and A. A. Al-Saleh, “Corneal spherical aberration and its impact on choosing an intraocular lens for cataract surgery”. *Saudi Journal of Ophthalmology*, 28: 274-280, 2014. DOI: https://doi.org/10.1016/j.sjopt.2014.06.005.

[3] M. P. Weikert, A. Golla, and L. Wang, "Astigmatism induced by intraocular lens tilt evaluated via ray tracing". *Journal of Cataract & Refractive Surgery*, 44: 745-749, 2018. DOI: https://doi.org/10.1016/j.jcrs.2018.04.035.

[4] A. Jóźwik, J. Nowak, D. Siedlecki, M. Zając, and J. Zarówny, "Retinal images in optomechanical eye model with monofocal intraocular lens". *Optica Applicata*, 41:593-605, 2011.

[5] K. H. Wan, A. C. Au, W. N. Kua, A. L. Ng, G. P. Cheng, N. M. Lam, and V. W. Chow, "Enhanced monofocal versus conventional monofocal intraocular lens in cataract surgery: a meta-analysis". *Journal of Refractive Surgery*, 38: 538-546, 2022. DOI: https://doi.org/10.3928/1081597X-20220707-01.

[6] J. L. Alio, A. B. Plaza-Puche, R. Férnandez-Buenaga, J. Pikkel, and M. Maldonado, "Multifocal intraocular lenses: an overview". *Survey of ophthalmology*, 62: 611-634, 2017. DOI: https://doi.org/10.1016/j.survophthal.2017.03.005.

[7] D. R. Breyer, H. Kaymak, T. Ax, F. T. Kretz, G. U. Auffarth, and P. R. Hagen, "Multifocal intraocular lenses and extended depth of focus intraocular lenses". *Asia-Pacific Journal of Ophthalmology*, 6:339-349, 2017. DOI: https://doi.org/10.22608/APO.2017186.

[8] M. Kaur, F. Shaikh, R. Falera, and J. S. Titiyal, "Optimizing outcomes with toric intraocular lenses". *Indian journal of ophthalmology*, 65:1301-1313, 2017. DOI: https://doi.org/10.4103/ijo.IJO_810_17.

[9] L. Kessel, J. Andresen, B. Tendal, D. Erngaard, P. Flesner, and J. Hjortdal, "Toric intraocular lenses in the correction of astigmatism during cataract surgery: a systematic review and meta-analysis". *Ophthalmology*, 123:275-286, 2016. DOI: https://doi.org/10.1016/j.ophtha.2015.10.002.

[10] M. Packer, I. H. Fine, and R. S. Hoffman, "Aspheric intraocular lens selection based on corneal wavefront". *Journal of Refractive Surgery*, 25:12-20, 2009. DOI: https://doi.org/10.3928/1081597X-20090101-03.

[11] R. Montés-Micó, T. Ferrer-Blasco, and A. Cerviño, "Analysis of the possible benefits of aspheric intraocular lenses: review of the literature". *Journal of Cataract & Refractive Surgery*, 35:172-181, 2009. DOI: https://doi.org/10.1016/j.jcrs.2008.09.017

[12] B. Cochener, A. Lafuma, B. Khoshnood, L. Courouve, and G. Berdeaux, "Comparison of outcomes with multifocal intraocular lenses: a meta-analysis." *Clinical Ophthalmology*, **5**:45-56, 2011. DOI: https://doi.org/10.2147/OPTH.S14325.

[13] K. L. Waltz, K. Featherstone, L. Tsai, and D. Trentacost, "Clinical outcomes of TECNIS toric intraocular lens implantation after cataract removal in patients with corneal astigmatism." *Ophthalmology*, 122(1):39-47, 2015. DOI: https://doi.org/10.1016/j.ophtha.2014.06.027.

[14] P. A. Piers, H. A. Weeber, P. Artal, and S. Norrby, "Theoretical comparison of aberration-correcting customized and aspheric intraocular lenses." *Journal of Refractive Surgery*, 23(4):374–384, 2007. DOI: https://doi.org/10.3928/1081-597X-20070401-10.

[15] X. Liu, M. Yu, Y. Huang, Q. Li, and W. Wu, "Intraocular lens tilt and decentration after cataract surgery with and without primary posterior continuous curvilinear capsulorhexis." Journal of Cataract & Refractive Surgery, 49(5):492–498, 2023. DOI: https://doi.org/10.1097/j.jcrs.0000000000001152.

[16] J. I. Fernández-Vigo, L. De-Pablo-Gómez-de-Liaño, I. Almorín-Fernández-Vigo, B. De-Pablo-Gómez-de-Liaño, A. Macarro-Merino, J. García-Feijóo, and J. Á. Fernández-Vigo, "The clinical usefulness of evaluating the lens and intraocular lenses using optical coherence tomography: an updated literature review." *Journal of Clinical Medicine*, 13(23):7070, 2024. DOI: https://doi.org/10.3390/jcm13237070.

[17] Y. Y. Jeon, N. Park, H. Lee, K. S. Eah, J. Han, H. S. Chung, and H. Lee, "Analysis of intraocular lens tilt and decentration after cataract surgery in eyes with high myopia using anterior segment optical coherence tomography." *Scientific Reports*, **14**:27987, 2024. DOI: https://doi.org/10.1038/s41598-024-78759-8.

[18] J. Pérez-Gracia, F. J. Ávila, J. Ares, J. A. Vallés, and L. Remón, "Misalignment and tilt effect on aspheric intraocular lens designs after corneal refractive surgery." *PLoS ONE*, 15(12):e0243740, 2020. DOI: https://doi.org/10.1371/journal.pone.0243740.

[19] P. Kanclerz, N. Bazylczyk, K. Przewłócka, R. Khoramnia, D. A. Atchison, and R. Tuuminen, "Risk factors for corneal monochromatic aberrations and implications for multifocal and extended depth-of-focus intraocular lens implantation." *Journal of Refractive Surgery*, 40(6):e420–e434, 2024. DOI: https://doi.org/10.3928/1081597X-20240416-01.

[20] H. Ye, K. Zhang, J. Yang, and Y. Lu, "Changes of corneal higher-order aberrations after cataract surgery." *Optometry and Vision Science*, 91(10):1244–1250, 2014. DOI: https://doi.org/10.1097/OPX.0000000000000362.

[21] L. M. Rodríguez, L. S. Tielas, A. Sánchez-Lozano, L. García-Onrubia, G. Velarde-Rodríguez, M. Á. Faria-Ribeiro, and N. Alejandre-Alba, "Clinical impact of intraocular lens tilt and decentration on visual outcome in patients undergoing cataract surgery." *Acta Ophthalmologica*, 103, 2025. DOI: https://doi.org/10.1111/aos.17000.

[22] J. B. Ale, "Intraocular lens tilt and decentration: a concern for contemporary IOL designs." *Nepalese Journal of Ophthalmology*, **3**(1):68–77, 2011. DOI: https://doi.org/10.3126/nepjoph.v3i1.4281.

[23] T. Oshika, M. Inamura, Y. Inoue, T. Ohashi, T. Sugita, Y. Fujita, and S. Nakano, "Incidence and outcomes of repositioning surgery to correct misalignment of toric intraocular lenses." *Ophthalmology*, **125**(1):31–35, 2018. DOI: https://doi.org/10.1016/j.ophtha.2017.07.004..

[24] H. A. Hashim and M. F. Mohammed, "Design and modeling of corneal aberration correction with diffractive IOL based on ZEMAX." *Results in Optics*, **11**:100398, 2023. DOI: https://doi.org/10.1016/j.rio.2023.100398.

[25] [25] H. L. Liou and N. A. Brennan, “Anatomically accurate, finite model eye for optical modeling.” Journal of the Optical Society of America A, 14(8):1684–1695, 1997. DOI: https://doi.org/10.1364/JOSAA.14.001684.

[26] M. Ranjbaran, K. Sangari, and S. Jalali, “Simulation model for advanced astigmatism corrective eyeglasses and contact lenses.” *Journal of Modern Optics*, **70**:1004–1013, 2023. DOI: https://doi.org/10.1080/09500340.2024.2379970.

[27] K. C. Shih, R. H. K. Tse, Y. T. Y. Lau, and T. C. Y. Chan, “Advances in corneal imaging: current applications and beyond.” *Asia-Pacific Journal of Ophthalmology*, **8**(2):105–114, 2019. DOI: https://doi.org/10.22608/APO.2018537.

[28] I. Abuallut, A. Ageeli, M. Shami, M. Bosaily, A. Majrashi, S. Shabaan, M. Moafa, W. Zakri, A. Abdulazim, and W.Barakat., “Keratoconus detected by corneal topography in patients seeking refractive surgery in Jazan region, Saudi Arabia: a retrospective cross-sectional study.” *Annals of Medicine and Surgery*, 79:103790, 2022. DOI: https://doi.org/10.1016/j.amsu.2022.103790

[29] J. H. Castillo, R. Hanna, E. Berkowitz, and B. Tiosano, “Wavefront analysis for keratoconus.” *International Journal of Keratoconus and Ectatic Corneal Diseases*, **3**(2):76, 2014. DOI: https://doi.org/10.5005/jp-journals-10025-1083.

[30] S. Mohan, M. Rajan, S. Singh, A. Bhirud, and S. Annavajjhala, “Wavefront analysis: an additional tool for detection of keratoconus.” *TNOA Journal of Ophthalmic Science and Research*, **55**(3):177–181, 2017. DOI: https://doi.org/10.4103/tjosr.tjosr_25_17.

[31] H. Hashemi, A. Beiranvand, A. Yekta, A. Maleki, N. Yazdani, and M. Khabazkhoob, “Pentacam top indices for diagnosing subclinical and definite keratoconus.” *Journal of Current Ophthalmology*, **28**(1):21–26, 2016. DOI: https://doi.org/10.1016/j.joco.2016.01.009.

[32] B. C. Platt and R. Shack, “History and principles of Shack–Hartmann wavefront sensing.” *Journal of Refractive Surgery*, 17(5):S573–S577, 2001. DOI: https://doi.org/10.3928/1081-597X-20010901-13.

[33] J. Marsack, A. Roorda, W. L. Miller, J. A. Jackson, N. E. Leach, and R. A. Applegate, “Development of a Shack–Hartmann wavefront sensor for a study of keratoconus.” *Investigative Ophthalmology & Visual Science*, **44**(13):4084, 2003.

[34] M. Ranjbaran, “Simulation model to study the impact of presbyopia on Shack–Hartmann wavefront maps.” *Journal of Optics*, 1–9, 2025. DOI: https://doi.org/10.1007/s12596-025-02851-z.

[35] M. Ranjbaran and R. Moradi, “Analysis of refractive errors using Shack–Hartmann wavefront sensor simulation.” *Indian Journal of Physics*, 1–9, 2025. DOI: https://doi.org/10.1007/s12648-025-03763-1.

[36] R. Yağcı, F. Uzun, S. Acer, and I. F. Hepşen, "Comparison of visual quality between aspheric and spherical intraocular lenses." *European Journal of Ophthalmology*, 24(5):688–692, 2014. DOI: https://doi.org/10.5301/ejo.5000452.

[37] J. Zvornicanin, E. Cabric, V. Jusufovic, Z. Musanovic, and E. Zvornicanin, "Use of the toric intraocular lens for keratoconus treatment." *Acta Informatica Medica*, 22(2):139-141, 2014. DOI: https://doi.org/10.5455/aim.2014.22.139-141

[38] K. Allard and M. Zetterberg, "Implantation of toric intraocular lenses in patients with cataract and keratoconus: a case series." *International Medical Case Reports Journal*, 11:185–191, 2018. DOI: https://doi.org/10.2147/IMCRJ.S174315.

[39] D. Farideh, S. Azad, N. Feizollah, N. Sana, A. Cyrus, G. Mohammad, and B. R. Alireza, "Clinical outcomes of new toric trifocal diffractive intraocular lens in patients with cataract and stable keratoconus: six months follow-up." Medicine, 96(12):e6340, 2017. DOI: https://doi.org/10.1097/MD.0000000000006340.

[40] Z. Ashena, S. Maqsood, S. N. Ahmed, and M. A. Nanavaty, "Effect of intraocular lens tilt and decentration on visual acuity, dysphotopsia and wavefront aberrations." *Vision*, 4(3):41, 2020. DOI: https://doi.org/10.3390/vision4030041.

[41] N. Hirnschall, N., T. Buehren, F. Bajramovic, M. Trost, T. Teuber, and O. Findl, "Prediction of postoperative intraocular lens tilt using swept-source optical coherence tomography." *Journal of Cataract & Refractive Surgery*, 43(6):732–736, 2017. DOI: https://doi.org/10.1016/j.jcrs.2017.01.026.

[42] B. S. Lee and D. F. Chang, "Comparison of the rotational stability of two toric intraocular lenses in 1273 consecutive eyes." *Ophthalmology*, 125(9):1325–1331, 2018. DOI: https://doi.org/10.1016/j.ophtha.2018.02.012.

[43] X. Y. Chen, Y. C. Wang, T. Y. Zhao, Z. Z. Wang, and W. Wang, "Tilt and decentration with various intraocular lenses: a narrative review." *World Journal of Clinical Cases*, 10(12):3639–3651, 2022. DOI: https://doi.org/10.12998/wjcc.v10.i12.3639.

[44] T. Eppig, K. Scholz, A. Löffler, A. Meßner, and A. Langenbucher, "Effect of decentration and tilt on the image quality of aspheric intraocular lens designs in a model eye." *Journal of Cataract & Refractive Surgery*, 35(6):1091–1100, 2009. DOI: https://doi.org/10.1016/j.jcrs.2009.01.034.

[45] W. N. Charman, R. Montés-Micó, and H. Radhakrishnan, "Problems in the measurement of wavefront aberration for eyes implanted with diffractive bifocal and multifocal intraocular lenses." *Journal of Refractive Surgery*, 24(3):280–286, 2008. DOI: https://doi.org/10.3928/1081597X-20080301-10.

[46] J. Schwiegerling and E. DeHoog, "Problems testing diffractive intraocular lenses with Shack–Hartmann sensors." *Applied Optics*, 49(16):D62–D68, 2010. DOI: https://doi.org/10.1364/AO.49.000D62.